Silver Quantum Cluster (Ag_9)-Grafted Graphitic Carbon Nitride Nanosheets for Photocatalytic Hydrogen Generation and Dye Degradation

ARTICLE *in* CHEMISTRY - A EUROPEAN JOURNAL · MAY 2015

Impact Factor: 5.73 · DOI: 10.1002/chem.201500163

6 AUTHORS, INCLUDING:

Kishore Sridharan
National Institute of Technology Karnataka
28 PUBLICATIONS **144** CITATIONS
SEE PROFILE

Eunyong Jang
Hanyang University
8 PUBLICATIONS **56** CITATIONS
SEE PROFILE

Jung-Ho Lee
Hanyang University
135 PUBLICATIONS **1,472** CITATIONS
SEE PROFILE

Tae Joo Park
Hanyang University
108 PUBLICATIONS **733** CITATIONS
SEE PROFILE

ChemPubSoc Europe

DOI: 10.1002/chem.201500163

CHEMISTRY
A European Journal
Full Paper

Photocatalysts

Silver Quantum Cluster (Ag_9)-Grafted Graphitic Carbon Nitride Nanosheets for Photocatalytic Hydrogen Generation and Dye Degradation

Kishore Sridharan,[a] Eunyong Jang,[a, b] Jung Hyun Park,[c] Jong-Ho Kim,*[c] Jung-Ho Lee,*[c] and Tae Joo Park*[a, b]

Abstract: We report the visible-light photocatalytic properties of a composite system consisting of silver quantum clusters [$Ag_9(H_2MSA)_7$] (H_2MSA = mercaptosuccinic acid) embedded on graphitic carbon nitride nanosheets (AgQCs-GCN). The composites were prepared through a simple chemical route; their structural, chemical, morphological, and optical properties were characterized by using X-ray diffraction (XRD), energy dispersive X-ray spectroscopy, transmission electron microscopy, UV/Vis diffuse reflectance spectroscopy, and photoluminescence spectroscopy. Embedment of [$Ag_9(H_2MSA)_7$] on graphitic carbon nitride nanosheets (GCN) resulted in extended visible-light absorption through multiple single-electron transitions in Ag quantum clusters and an effective electronic structure for hydroxyl radical generation, which enabled increased activity in the photocatalytic degradation of methylene blue and methyl orange dye molecules compared with pristine GCN and silver nanoparticle-grafted GCN (AgNPs-GCN). Similarly, the amount of hydrogen generated by using AgQCs-GCN was 1.7 times higher than pristine GCN. However, the rate of hydrogen generated using AgQCs-GCN was slightly less than that of AgNPs-GCN because of surface hydroxyl radical formation. The plausible photocatalytic processes are discussed in detail.

Introduction

The discovery of the light-driven water-splitting reaction has made a massive impact on semiconductor photocatalysis research, which continues to remain vital owing to its huge potential in solar fuel production and environmental remediation.[1] Titanium oxide (TiO_2), a wide band gap semiconductor ($E_g \approx 3.2$ and ≈ 3.0 eV for anatase and rutile phase, respectively) has been investigated extensively for photocatalytic applications due to high photoactivity, excellent chemical and thermal stability, easy synthesis, low toxicity, and abundant availability.[2] However, recently, graphitic carbon nitride ($g\text{-}C_3N_4$, referred hereafter as GCN), an organic polymer with a narrow band gap of ≈ 2.7 eV has been treated as the successor of TiO_2 because of its similarity in properties such as high chemical stability, easy synthesis, and availability of cost effective precursors.[3] Unlike TiO_2, GCN is visible-light active but suffers from a high rate of electron-hole pair recombination.[4] Therefore, many attempts have been made to couple GCN with different nanostructured materials for enhancing the separation of charge carriers and improving its photocatalytic activity.[5]

Noble metal (Ag, Au, and Pt) nanoparticles (NPs) have attracted tremendous research interest in photocatalysis for solar water-splitting and photodecomposition of organic pollutants.[6] Noble metal NPs-coupled semiconductor nanostructures were found to exhibit improved solar energy conversion efficiency for photocatalytic and photovoltaic device applications.[7] Light incident on the noble metal NPs stimulates the collective oscillation of surface electrons through the surface plasmon resonance (SPR) effect.[8] Metal NPs offer a direct electron transfer (DET) to the conduction band of the semiconductor through SPR, which also enhances the light absorption, light scattering, and charge separation of the coupled semiconductor nanostructures.[9]

On the other hand, extremely small-sized noble metal particles (< 2 nm), which are commonly referred as nanoclusters or quantum clusters (QCs), exhibit unique chemical, optical and electronic properties because of the drastic changes in size and atomic structure arrangement. Typically, metal QCs exhibiting molecular-like properties are protected by thiolate ligand

[a] Dr. K. Sridharan, E. Jang, Prof. T. J. Park
Department of Materials Science and Engineering
Hanyang University, Ansan
Gyeonggi-do 426-791 (Republic of Korea)
E-mail: tjp@hanyang.ac.kr

[b] E. Jang, Prof. T. J. Park
Department of Advanced Materials Engineering
Hanyang University, Ansan
Gyeonggi-do 426-791 (Republic of Korea)

[c] J. H. Park, Prof. J.-H. Kim, Prof. J.-H. Lee
Department of Chemical Engineering
Hanyang University, Ansan
Gyeonggi-do 426-791 (Republic of Korea)
E-mail: kjh75@hanyang.ac.kr
jungho@hanyang.ac.kr

Supporting information for this article is available on the WWW under http://dx.doi.org/10.1002/chem.201500163.

groups, which control the number of metal atoms. Stabilized metal QCs exhibiting molecular-like property are therefore named along with the thiol group, for example, $[Au_{144}(SR)_{60}]$, in which Au_{144} denotes the number of gold metal atoms in the cluster protected by 2-phenylethanethiolate ligand (SR). Recently, noble metal QCs have attracted enormous research attention because of their discrete energy levels, which have already found applications in bioimaging, catalysis, nanoelectronics, nanophotonics, and sensing.[10] Unlike semiconductor quantum dots, metal quantum clusters are non-toxic and environmentally friendly, which make them attractive candidates for environmental remediation and hydrogen production through photocatalysis.[11] Some of the reports on the usage of metal quantum clusters for photocatalysis are summarized as follows. Chen et al. studied the electron-transfer properties of Ag NPs capped with Ag_8 QCs and confirmed the capability of QCs to photocatalytically reduce methyl viologen molecules.[12] Yu et al. reported enhanced visible-light photocatalytic activity in the degradation of methyl orange dye molecules by using Au_{25} QCs/TiO_2 composites.[13] Attia et al. demonstrated the capability of Ag_3 QCs to catalyze the anisotropic growth of gold nanorods for photocatalytic hydrogen production.[14] Similarly, Chen et al. reported the visible-light-induced hydrogen generation by using glutathione-capped gold nanoclusters as sensitizers.[15] These reports have so far highlighted the potential of thiolate-protected metal quantum clusters for photocatalytic dye degradation and hydrogen generation. However, the photocatalytic activity studies on dye degradation, as well as hydrogen generation, by using a composite formed by grafting silver quantum clusters on graphitic carbon nitride nanosheets is seldom reported.

Herein, we have synthesized a composite consisting of thiol-protected nine atom silver QCs having a molecular structure with composition $[Ag_9(H_2MSA)_7]$ (H_2MSA = mercaptosuccinic acid), which were grafted on GCN (referred hereafter as AgQCs-GCN) through a facile synthetic technique. The visible-light photocatalytic activity of AgQCs-GCN composites was studied by monitoring the degradation of dye molecules and through hydrogen generation. Compared with GCN and Ag NPs-grafted GCN (AgNPs-GCN), the rate of dye degradation using AgQCs-GCN was found to be higher. On the other hand, the yield of hydrogen generation by using AgNPs-GCN was slightly higher than that of AgQCs-GCN. A plausible mechanism for enhancement in the photocatalytic activity of AgQCs-GCN was investigated as well.

Results and Discussion

The XRD patterns of AgQCs, AgQCs-GCN, AgNPs-GCN, and pristine Ag NPs samples are shown in Figure 1. XRD peaks formed at $2\theta = 27.4^\circ$ in both the AgQCs-GCN and AgNPs-GCN represent the (002) plane of GCN. Because of the small loading of Ag NPs and Ag QCs in GCN, no significant diffraction peaks corresponding to Ag were observed. The intense XRD peaks of as-synthesized Ag NPs can be indexed to the face-centered cubic (fcc) structure of Ag (JCPDS card #04-04783).On the contrary, the XRD pattern of Ag QCs exhibits a broad peak with

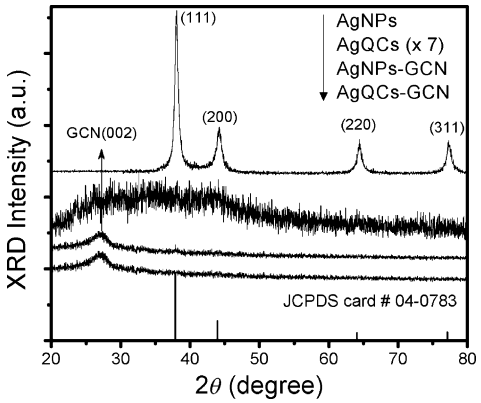

Figure 1. XRD patterns of AgQCs, AgQCs-GCN, and AgNPs-GCN samples in comparison to pristine Ag NPs.

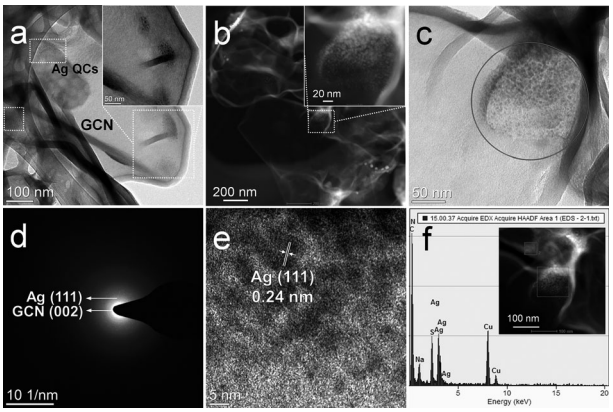

Figure 2. a) TEM image of the synthesized AgQCs-GCN; the areas marked by boxes indicate the presence of Ag QCs and the inset shows the presence of Ag QCs embedded in GCN; b) HAADF-STEM image of AgQCs-GCN, the inset clearly indicates the presence of the Ag clusters; c) TEM image of AgQCs-GCN, the encircled area indicates the area from which the d) SAED pattern is obtained. The bright ring at the center depicts the presence of the (002) plane of GCN, whereas the outer ring can be assigned to the (111) plane of Ag QCs; e) HRTEM image of AgQCs-GCN, the d-spacing value was estimated to 0.24 nm, which can be assigned to the (111) plane of Ag; f) EDS spectra acquired from the area marked in the HAADF-STEM image shown in the inset. The elemental peaks of Ag, Na, S, C, and N confirm the presence of Ag quantum clusters and GCN.

a center at $2\theta = 38^\circ$, which clearly indicates its poor crystallinity; this is in agreement with the literature.[10a,b] Figure 2a shows a typical TEM image of the AgQCs-GCN sample, in which the areas marked by boxes indicate the presence of Ag QCs embedded on GCN. The high-angle annular dark field scanning transmission electron microscopy (HAADF-STEM) image in Figure 2b clearly indicates the presence of Ag QCs. The atomic size distribution of the Ag QCs is clearly observed in the inset of Figure 2b. The selected area electron diffraction (SAED) pattern (Figure 2d) was obtained from an area marked in the TEM image presented in Figure 2c. The bright central ring with high intensity indicates the dominant presence of the (002) plane of GCN, whereas the low intensity ring indicates the (111) plane of Ag, which are consistent with XRD results. An atomic spacing value of 0.24 nm in the HRTEM image

of Figure 2e also corresponds to the (111) plane of Ag. The energy dispersive spectroscopy (EDS) result of AgQCs-GCN sample in Figure 2f was acquired from the area of the HAADF-STEM image shown in the inset. The elemental peaks from C, N, Ag, S, and Na reveal the existence of GCN and Ag QCs. The atomic ratio between Ag and S, which is expected to be 1:0.77 for Ag_9 QCs, is consistent with the reports in the literature.[10a] Furthermore, the EDS results from TEM are in accordance with those obtained through scanning electron microscopy (SEM; as shown in Figure S1 in the Supporting Information). Next, we examined the structure of AgNPs-GCN. Figure 3a and 3b show the TEM and HAADF-STEM images of AgNPs-GCN sample, respectively. The average size of Ag NPs from Figure 3a is about 7 nm. The embedded Ag NPs on the surface of GCN are more clearly observed in the HAADF-STEM image of Figure 3b. The EDS spectra in Figure 3c, acquired by scanning the area marked in the inset HAADF-STEM image, confirms that the bright particles are AgNPs.

UV/Vis absorption spectra of the as-synthesized Ag NPs and $[Ag_9(H_2MSA)_7]$ QCs solutions were recorded to additionally verify their formation. The Ag NPs exhibit a clear plasmonic absorption peak at 390 nm, whereas Ag_9 QCs show multiple optical absorption peaks, indicating quantum size effect (see Figure S2 in the Supporting Information).[10a] The optical photographs of the AgQCs-GCN, AgNPs-GCN, and GCN are shown in Figure 4a, 4b and 4c, respectively. Figure 4d shows the absorbance spectra of the prepared samples obtained by using diffuse reflectance spectroscopy (DRS). Compared with GCN, both AgNPs-GCN and AgQCs-GCN showed improved visible light absorbance. AgNPs-GCN displayed maximum absorbance with a peak at ≈385 nm, which can be attributed to the SPR effect of Ag NPs.[5b] Interestingly, only AgQCs-GCN exhibited an extended visible-light absorbance (>500 nm); this is because of the critical size of the Ag QCs, which results in multiple optical absorption because of the discrete quantum confined electronic transitions, and will be discussed later from the viewpoint of photocatalytic activity. Figure 4e shows the E_g values of the samples that were estimated by drawing tangent lines in the plots of the square root of the Kubelka–Munk function ($\alpha^{1/2}$) against photon energy. The estimated E_g values were ≈2.10, ≈2.45, and ≈2.65 eV for AgQCs-GCN, AgNPs-GCN, and GCN, respectively. The reduction in the estimated E_g value of AgQCs-GCN compared with AgNPs-GCN is due to the various electron transitions by the quantum confinement effect of Ag_9 QCs.[10a]

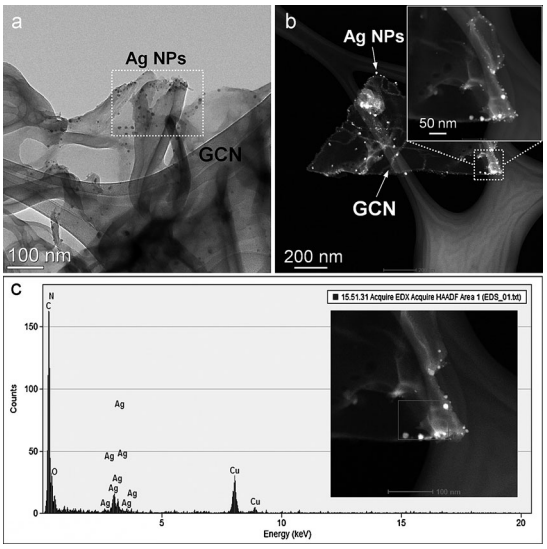

Figure 3. a) TEM and b) HAADF-STEM images of the as-synthesized AgNPs-GCN, indicating the presence of Ag NPs grafted in the GCN sheets; c) EDS spectra obtained from the area marked in the HAADF-STEM image shown in the inset. The presence of the elemental peaks from C, N, and Ag confirm the presence of GCN and Ag NPs. The Cu peak arises from the carbon-coated copper grid, which is used as the substrate during TEM analysis.

The photocatalytic performances of the prepared samples were evaluated by testing the photocatalytic degradation of some colored contaminants (organic dye molecules) in waste water. It was recently reported by Bootharaju and Pradeep,[16] that ligand-protected Ag QCs can selectively remove cationic dyes because of the favorable electrostatic interaction (between dye molecules and clusters). But, the removal of anionic

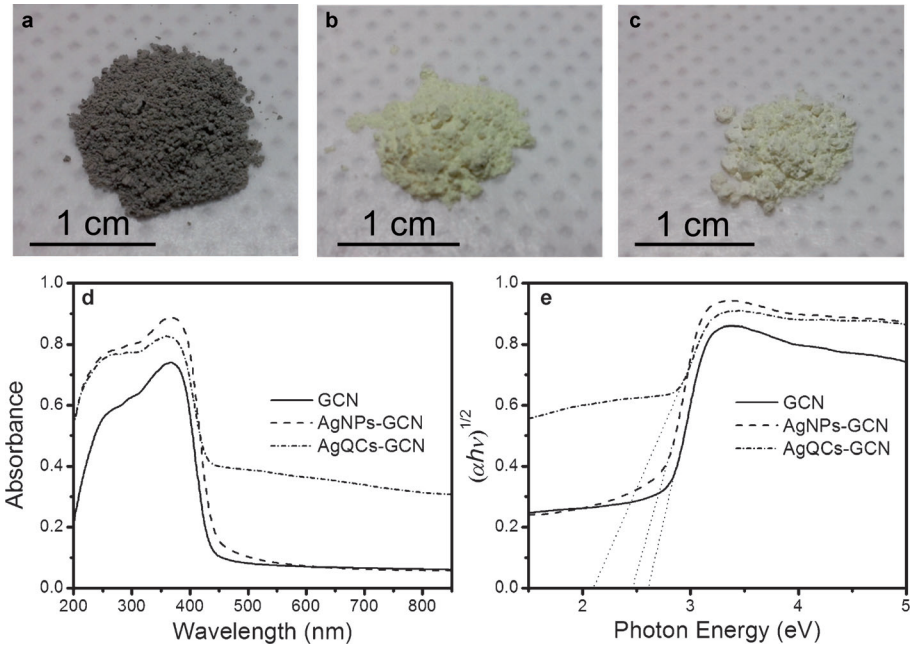

Figure 4. Color photographs of the a) AgQCs-GCN, b) AgNPs-GCN, and c) GCN; d) Optical absorbance spectra of the synthesized samples and e) Tauc plots constructed by using the Kubelka–Munk function of absorbance against photon energy. The tangent lines touching the energy axis indicate the energy band gap values.

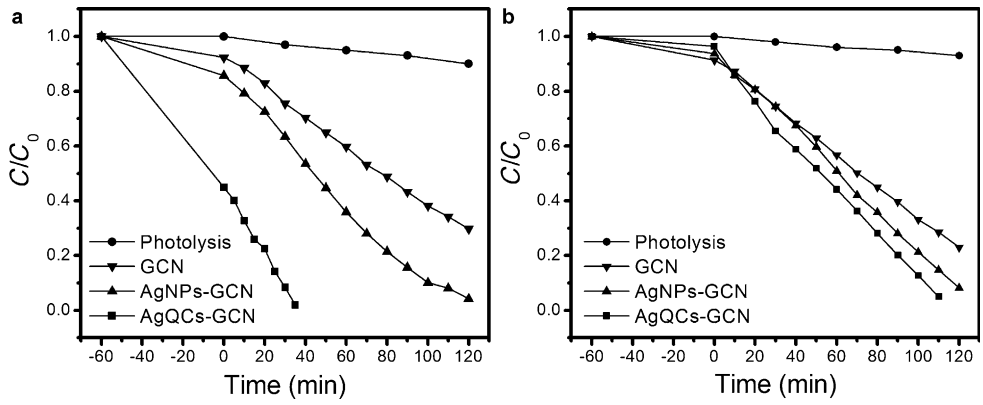

Figure 5. Photocatalytic degradation of a) methylene blue and b) methyl orange dye molecules in the presence of the prepared samples.

dye molecules was a failure because of the strong electrostatic repulsion between anionic dye molecules and Ag QCs. Therefore, to separate the adsorptive behavior of Ag QCs from the photocatalytic activity, both cationic (methylene blue, MB) and anionic (methyl orange, MO) dyes were used as model contaminants. Figure 5 depicts the visible-light photodegradation of MB and MO dye solutions using the prepared catalysts. As shown in Figure 5a and 5b (●), the photolysis of MB and MO dyes in the absence of the catalysts under visible light is negligible. Interestingly, the rate of photodegradation of MB dyes by AgQCs-GCN was approximately three times faster than that of MO dyes, which can be attributed to the electrostatic attraction between S atoms in MB dye molecules and Ag QCs clusters. On the other hand, a strong electrostatic repulsion arises between MO and Ag QCs; the sulfonic group of MO has a high electronegative center and it is more electron-withdrawing than that of the carboxylic groups present in Ag QCs. Therefore, this resulted in a low adsorption value, which considerably reduced the photodegradation rate.

It is worth noting that the electrostatic forces discussed above are applicable only for Ag QCs (due to the presence of ligands) and hence the photocatalytic activities of GCN and AgNPs-GCN had no special effect based on the dye type (anionic/cationic). Meanwhile, the photodegradation in the presence of AgQCs-GCN was found to be higher than that of GCN and AgNPs-GCN for both MO and MB dyes, which is explained as follows. In general, when light is irradiated on a semiconductor, electrons (e^-) are excited to the conduction band (CB), creating a hole (h^+) on the valence band (VB). These photogenerated electrons react with O_2 molecules to form superoxide radical anions (O_2^-) and the photoinduced holes react with the surface-bound hydroxyl ions (OH^-) to produce hydroxyl free-radicals ($^{\bullet}OH$).[5b,17] The plausible mechanism of photocatalytic dye degradation in the presence of AgNPs coupled with GCN is shown in Scheme 1a and that of $[Ag_9(H_2MSA)_7]$ (Ag QCs) coupled with GCN is shown in Scheme 1b.

For GCN, the energy level positions for the lowest unoccupied molecular orbital (LUMO) and the highest occupied molecular orbital (HOMO) have been found to be −1.13 and +1.57 eV, respectively.[18] When GCN is coupled with Ag NPs (AgNPs-GCN), a metal/semiconductor interface is established because of the work function difference between Ag NPs and GCN, which creates a Schottky barrier (Scheme 1a). The SPR effect of Ag NPs induces the strong local electromagnetic field, which in turn enhances the photon-induced charge carriers generation within GCN.[5b,19] Therefore, the inclusion of Ag NPs provide sufficient time for the photogenerated electrons (e^-) in GCN to participate in multiple-electron reduction of oxygen by charge (electron) transfer from GCN to Ag NPs, which in turn leads to the indirect generation of $^{\bullet}OH$ radicals [Eq. (1)], which are responsible for the degradation of dye molecules.[19]

$$O_2 + 2H^+ + 3e^- \rightarrow {}^{\bullet}OH + OH^- \quad (1)$$

However, the HOMO level potential of bare GCN is more negative than the standard redox potential of $OH^-/^{\bullet}OH$ (2.27 V vs. SHE) and hence the photogenerated holes (h^+) cannot oxidize OH^- to generate $^{\bullet}OH$ radicals.[1a,5b,20] The failure of this oxidation reaction is schematically depicted in Scheme 1a with a strike out symbol.

On the other hand, AgQCs-GCN is a coupled semiconductor composite, which forms a semiconductor heterojunction because of the difference in the conduction band (CB/LUMO) and valance band (VB/HOMO) redox energy levels, which improves the separation of charge carriers. Therefore, an improved photocatalytic activity can obviously be expected in AgQCs-GCN. Herein, the strong quantum confinement effect in Ag QCs enables it to exhibit multiple molecular-like single-electron transi-

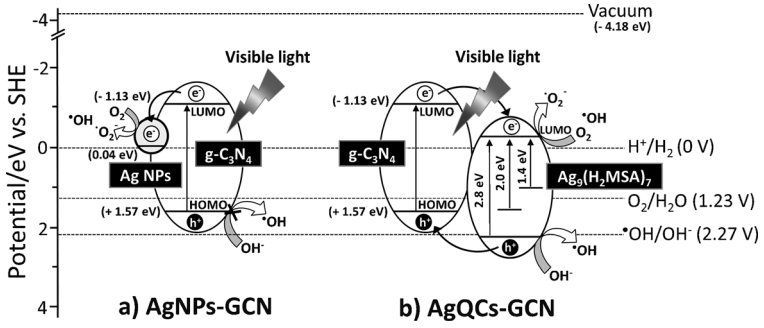

Scheme 1. Mechanism of visible light photocatalytic degradation of MB/MO dye molecules in the presence of a) silver nanoparticles grafted in graphitic carbon nitride nanosheets (AgNPs-GCN) and b) silver quantum clusters grafted in graphitic carbon nitride (AgQCs-GCN).

tions.[13] The absorption peaks of Ag QCs formed at 450, 625, and 886 nm can be related to Kohn–Sham molecular orbitals, which are ascribed to various electron transitions from the HOMO to the LUMO level,[10a] (see Figure S2 in the Supporting Information and Scheme 1 b), which induced the extended optical absorbance in AgQCs-GCN as seen in Figure 4. Therefore, more electrons and holes are generated in AgQCs-GCN under visible-light irradiation than in AgNPs-GCN as depicted in Scheme 1 b. Recently, the potential of $[Au_{25}(SR)_{18}]$ (25 atom gold clusters) was reported to be more negative than the CB potential of TiO_2.[13] So it would be reasonable to assume that the potential of Ag_9 QCs will be similar or less than that of the potential of $[Au_{25}(SR)_{18}]$, in which the HOMO level is more positive than the standard redox potential of $OH^-/^{\bullet}OH$.

The photogenerated electrons in the LUMO of GCN are favorably transferred to the LUMO of Ag QCs through the heterojunction interface, which are then transferred to molecular oxygen to efficiently generate superoxide radical anions $^{\bullet}O_2^-$.[21] This contributes to the production of singlet oxygen ($^1O_2$), which aids the degradation of dye molecules.[22] In addition, the photogenerated holes in the VB of Ag QCs can directly generate $^{\bullet}OH$ free radicals as per Equation (2), which are also responsible for the degradation of the dye molecules. The excess holes are efficiently transferred to GCN through the heterojunction, which eventually leads to recombination. These two different types of photocatalytically generated reactive oxygen species ($^{\bullet}O_2^-$, $^{\bullet}OH$) lead to the enhanced photoactivity of AgQCs-GCN in the degradation of the dye molecules.

$$h^+_{HOMO} + OH^- \rightarrow {}^{\bullet}OH \text{ (direct degradation)} \quad (2)$$

Furthermore, AgQCs-GCN exhibited an improved surface area of 38.3 $m^2 g^{-1}$ (see Figure S3 in the Supporting Information) compared with those of AgNPs-GCN ($S_{BET} = 30.3\ m^2 g^{-1}$) and GCN ($S_{BET} = 27.7\ m^2 g^{-1}$). Therefore, the improved surface area of AgQCs-GCN along with its apt E_g value of ≈ 2.1 eV, enabling it to efficiently function under the visible region of the solar spectrum, are the factors contributing to the enhanced photocatalytic dye degradation.

The PL spectra of the photocatalysts excited at 350 nm is shown in Figure 6. The main emission peak for GCN observed

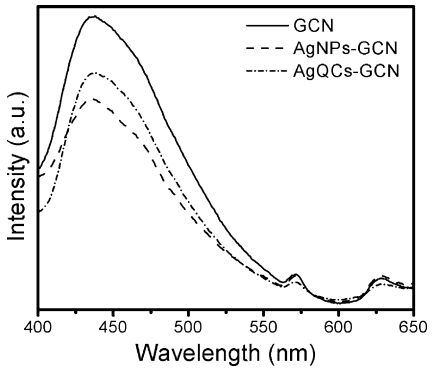

Figure 6. Photoluminescence spectra of GCN, AgNPs-GCN, and AgQCs-GCN, recorded at an excitation wavelength of 350 nm.

herein is consistent with those reported in the literature.[23] In general, the PL emission originates from the recombination of electron-hole pairs, and therefore the decrease in the PL emission intensity is due to the decreased rate of charge recombination. In the present case, the PL intensities are in the order GCN > AgQCs-GCN > AgNPs-GCN, which means the rate of electron-hole pair recombination is the highest in GCN, whereas it is the lowest in AgNPs-GCN. Even though the recombination rate of AgQCs-GCN is higher than that of AgNPs-GCN due to generation of the larger amount of holes, the combined action of the superoxide ($^{\bullet}O_2^-$) and hydroxyl radicals ($^{\bullet}OH$) enhanced its rate of dye degradation.[24] However, the higher rate of charge recombination in AgQCs-GCN resulted in lower rate of H_2 generation because in the hydrogen evolution reaction, electrons (e^-) play a major role in reducing H^+ ions to H_2 while the holes (h^+) are scavenged, which is discussed in the following section.

The amount of photocatalytic H_2 generated by using the GCN composites under simulated solar light irradiation for a period of 2 h is plotted in Figure 7. Control experiments con-

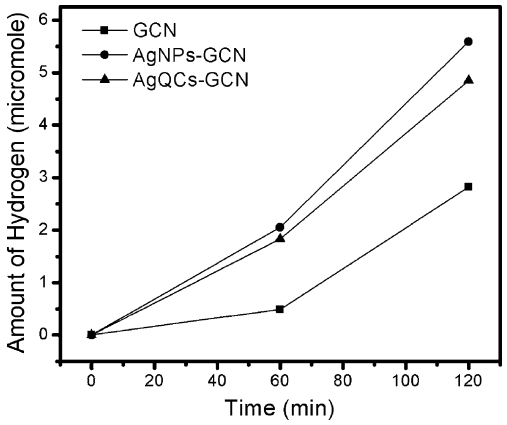

Figure 7. Amount of hydrogen generated in methanol suspension by using GCN, AgNPs-GCN, and AgQCs-GCN as the photocatalyst along with 1.0 wt% of Pt nanoparticles as the co-catalyst, under solar light irradiation.

ducted under the absence of either light or photocatalyst produced no appreciable amount of hydrogen, indicating that the evolution happens only through photocatalysis. As seen from Figure 7, the amount of H_2 generated by using GCN (2.82 μmol) was the lowest, whereas it was the highest for AgNPs-GCN (5.59 μmol). Although the amount of H_2 generated using AgQCs-GCN (4.85 μmol) was 1.7 times higher than that of GCN, it was slightly lower compared with that of AgNPs-GCN. To understand this difference, we need to understand the mechanism of photocatalytic H_2 generation using AgNPs-GCN, which is described in Equations (3)–(5).[23a]

$$AgNPs - GCN \xrightarrow{h\nu} AgNPs(e^-), Pt(e^-)/GCN(h^+) \quad (3)$$

$$AgNPs(e^-)/Pt(e^-) + 2H^+ \rightarrow AgNPs/Pt + H_2 \quad (4)$$

$$GCN(h^+) + CH_3OH + 6OH^- \rightarrow GCN + CO_2 + 5H_2O \quad (5)$$

As mentioned in the Experimental Section, before light illumination, the suspension containing the photocatalyst sample is completely deoxygenated (to avoid electron scavengers). Under these conditions (absence of electron scavengers), the Fermi level of both Pt NPs and Ag NPs can increase until it is pinned by the redox pair H^+/H_2.[14] Hence, the electrons (e^-) accumulated in Pt NPs and Ag NPs (transferred from LUMO level of GCN during light illumination by the formation of Schottky barrier) can effectively reduce H^+ to produce H_2 and the holes (h^+) formed at the HOMO level of GCN react with the sacrificial agent methanol (hole scavenger), which inhibits the recombination of the photogenerated charges.

Compared with AgNPs-GCN, the yield of H_2 evolution for AgQCs-GCN seems to be slightly lower (Figure 7, ▲). This may be because AgQCs can oxidize the surface-bound OH^- to form a hydroxyl radical, which eventually decreases their capability of oxidizing H_2O or CH_3OH to produce protons. Furthermore, the sulfur atoms in the thiolate ligand in AgQCs can react with Pt NPs, which may hinder its ability to reduce protons.[25] Therefore, the reduced amount of protons may be responsible for the lower yield of H_2 for AgQCs-GCN, but this deactivation step cannot occur in the case of AgNPs-GCN. In addition, the charge recombination rate is higher for AgQCs-GCN, even in the presence of methanol as the hole scavenger, because holes (h^+) are produced at the HOMO level of both GCN and Ag QCs (Scheme 1 b), as observed from the PL results (Figure 6). However, compared with GCN, the H_2 generation yield using AgQCs-GCN is significantly higher, which can be attributed to the synergistic effect of the heterojunction between Ag QCs and GCN, such that the electrons produced at the LUMO level of both GCN and Ag QCs are trapped by Pt NPs, at which H^+ is reduced to H_2. In the case of bare GCN, the yield of H_2 generation is the lowest because of the very quick recombination of charge carriers (as seen in Figure 6), which allows only a fraction of the electrons formed at the LUMO level of GCN to be trapped by the Pt NPs.[23a,26]

Conclusion

We have successfully demonstrated the simple method to synthesize nine atom silver cluster $[Ag_9(H_2MSA)_7]$-grafted graphitic carbon nitride nanosheets (AgQCs-GCN). XRD, EDS, and TEM analysis confirmed the formation of the composite samples. The optical properties were studied through UV/Vis DRS spectroscopy and the energy band gap values were estimated by using Kubelka–Munk theory. The AgQCs-GCN sample showed improved photocatalytic activity compared with pristine GCN for both dye degradation as well as hydrogen generation. The plausible reasons for the enhanced photocatalytic activity have been discussed through the enhanced absorbance originating from quantum confinement effect and a model depicting the effective electronic structure for the generation of hydroxyl radicals. Even though AgQCs-GCN exhibits a higher efficiency in dye degradation compared with AgNPs-GCN, the hydrogen generation yield for AgNPs-GCN was found to be slightly higher than that of AgQCs-GCN. This is due to the lower recombination rate and the suppressed surface hydroxyl radical formation. This study indicates that silver metal quantum clusters with semiconductor-like properties are potential candidates that can be further explored in the design and development of efficient photocatalysts for solar fuel generation application.

Experimental Section

Synthesis of AgQCs-GCN

Ag QCs-grafted GCN were typically prepared through a two-step approach. In step one, the precursors for the grafting reaction were prepared separately; GCN was prepared through pyrolysis of urea in a sealed crucible following the work of Liu et al.[3b] Ag_9QCs were prepared through a solid-state synthesis route under room temperature conditions.[10a] Typically, $AgNO_3$ (0.047 g) was ground well with H_2MSA (0.187 g). An orange powder (silver thiolate) was obtained, which was again ground well with $NaBH_4$ (0.050 g) to yield a brown powder. De-ionized water (15 mL) was then added slowly in drops to this mixture; a dark-colored solution (Ag QCs solution) was obtained as the product. An ethanolic dispersion of GCN was prepared by ultrasonicating GCN (0.020 g) in ethanol (20 mL) for a period of 30 min. In the second step, the Ag QCs solution (2 mL) was precipitated by dropping into the ethanolic GCN dispersion, under continuous stirring. The as-obtained silver clusters protected by thiol had a composition $[Ag_9(H_2MSA)_7]$. The final precipitate washed repeatedly with ethanol was dried in an oven at 80 °C for 12 h. The dried product was named AgQCs-GCN.

Synthesis of AgNPs-GCN

For a comparison, Ag NPs were also grafted in GCN, which were named AgNPs-GCN. In a typical process, GCN (0.020 g) was dispersed in de-ionized water (50 mL) and this solution was ultrasonicated for a period of 30 min. $AgNO_3$ (0.0021 g, 0.25 mM) and $Na_3C_6H_5O_7$ (0.0037 g, 0.25 mM), respectively, were added to this solution, under agitation. After 5 min under vigorous magnetic stirring, a freshly prepared solution of $NaBH_4$ (1.5 mL, 0.01 M) was added in drops. The color of the solution changed at once to yellow, indicating the formation of Ag sols. The final product (AgNPs-GCN), collected by repeated centrifugation using excess de-ionized water, was dried at 100 °C for 12 h.

Characterization

Powder X-ray diffraction (XRD) patterns of the prepared samples were obtained by using an X-ray diffractometer (Rigaku-Dmax 2500) with $Cu_{K\alpha}$ radiation ($\lambda = 0.15405$ nm, 40 kV, 100 mA). The samples were scanned in the range of $2\theta = 10$–$80°$. Morphology and energy dispersive X-ray spectroscopy (EDS) of the prepared samples were analyzed by using a MIRA3 TESCAN high-resolution scanning electron microscope (SEM) equipped with a high brightness Schottky field emission gun. High-resolution transmission electron microscopy (HRTEM), EDS, selected area electron diffraction pattern (SAED) analysis and high-angle annular dark-field scanning TEM (HAADF-STEM) were performed on a FEI Technai G2 F20 model microscope operated at 200 kV. Samples for TEM were prepared by dropping the sample solution dispersed in ethanol onto a carbon-coated copper grid. Surface areas of the samples were estimated by measuring the nitrogen adsorption-desorption isotherms on a Micrometrics ASAP2010 system. All the samples were degassed at 120 °C for 2 h before the surface area measurements. UV/Vis diffuse reflectance spectra (DRS) of the photocatalysts were

recorded on a JASCO V-550 UV/Visible spectrophotometer equipped with an integrating sphere (JASCO ISV-469), using a dedicated powder sample holder (JASCO PSH-001). UV/Vis absorption spectra of the liquid samples were measured using the same spectrophotometer. Photoluminescence (PL) spectra of the samples were measured at room temperature using a Flurolog-3 spectrofluorometer (Horiba Jobin Yvon) system, consisting of a CW 450 W Xenon short arc excitation source. Samples for PL were prepared by dispersing the powder samples in ethanol, with equivalent concentration.

Photocatalytic dye degradation

Reaction slurries for photocatalysis experiments were prepared by dissolving 50 mg of the photocatalyst powder sample in 200 mL of methylene blue (MB) and methyl orange (MO) dye solutions (concentration: 1×10^{-5} M), which was then stirred for 60 min in the dark to ensure dye adsorption on the surface of the catalyst. A Halogen lamp (100 W, HI-Spot 95) purchased from Osram Sylvania Inc., with UV-stop feature was used as the visible-light source. The reaction slurry was vigorously stirred during the photocatalytic reaction process. Aliquots were sampled at regular intervals of illumination time. The concentrations of the dye in the aliquots were determined from the maximum absorption wavelength using a UV/Vis spectrophotometer (JASCO V-550). The dye photodegradation percentages (C/C_0) were calculated according to decrease in the absorption peak of MB and MO dye with respect to irradiation time, in which C represents the change in concentration and C_0 is the initial dye concentration.

Photocatalytic hydrogen evolution

The photocatalytic activity of GCN composites for hydrogen evolution reaction was performed after deposition of platinum as a co-catalyst. In our experiment, 10 mg of GCN (AgNPs-GCN or AgQCs-GCN) was dispersed in 40 mL of a H_2O/CH_3OH solution (3:1) through ultrasonication. Then, 1.0 wt.% of K_2PtCl_4 was added to the solution under stirring while it was irradiated with UV light (300W, Raynics Korea) for 30 min. The GCN solution was added into a quartz reactor, which was sealed with a preassembled cap fitted with a pressure transducer and a septum. The solution was degassed with argon for 30 min to remove dissolved oxygen, before being illuminated using a solar simulator (Newport Corp., Irvine, CA USA) with AM 1.5 G radiation for 2 h. The evolved amount of H_2 was measured using gas chromatography (GC) (YL Instruments 6500GC) by injecting 200 μL of the gases collected from the headspace of the reactor into the GC instrument. The absolute amount of H_2 was calculated based on a calibration plot.

Acknowledgements

This work was supported by the National Research Foundation of Korea (NRF) grant funded by the Korea government (MEST) (No. 2012R1A2A2A01047579), and by the New & Renewable Energy of the Korea Institute of Energy Technology Evaluation and Planning (KETEP) grant (No. 20123010010160) funded by the Korea government Ministry of Knowledge Economy.

Keywords: dyes · hydrogen · nanosheets · quantum clusters · silver · UV/Vis spectroscopy

[1] a) A. Fujishima, T. N. Rao, D. A. Tryk, *J. Photochem. Photobiol. C* **2000**, *1*, 1–21; b) Z. Zou, J. Ye, K. Sayama, H. Arakawa, *Nature* **2001**, *414*, 625–627.
[2] a) A. L. Linsebigler, G. Lu, J. T. Yates, *Chem. Rev.* **1995**, *95*, 735–758; b) M. Pelaez, N. T. Nolan, S. C. Pillai, M. K. Seery, P. Falaras, A. G. Kontos, P. S. M. Dunlop, J. W. J. Hamilton, J. A. Byrne, K. O'Shea, M. H. Entezari, D. D. Dionysiou, *Appl. Catal. B* **2012**, *125*, 331–349.
[3] a) X.-H. Li, M. Antonietti, *Chem. Soc. Rev.* **2013**, *42*, 6593–6604; b) J. Liu, T. Zhang, Z. Wang, G. Dawson, W. Chen, *J. Mater. Chem.* **2011**, *21*, 14398–14401; c) S. Yang, Y. Gong, J. Zhang, L. Zhan, L. Ma, Z. Fang, R. Vajtai, X. Wang, P. M. Ajayan, *Adv. Mater.* **2013**, *25*, 2452–2456.
[4] a) P. Niu, L. Zhang, G. Liu, H.-M. Cheng, *Adv. Funct. Mater.* **2012**, *22*, 4763–4770; b) Y. Hou, Z. Wen, S. Cui, X. Guo, J. Chen, *Adv. Mater.* **2013**, *25*, 6291–6297.
[5] a) K. Sridharan, E. Jang, T. J. Park, *Appl. Catal. B* **2013**, *142–143*, 718–728; b) L. Ge, C. Han, J. Liu, Y. Li, *Appl. Catal. A* **2011**, *409–410*, 215–222; c) K. Sridharan, T. Kuriakose, R. Philip, T. J. Park, *Appl. Surf. Sci.* **2014**, *308*, 139–147.
[6] M. Xiao, R. Jiang, F. Wang, C. Fang, J. Wang, J. C. Yu, *J. Mater. Chem. A* **2013**, *1*, 5790–5805.
[7] a) S. T. Kochuveedu, Y. H. Jang, D. H. Kim, *Chem. Soc. Rev.* **2013**, *42*, 8467–8493; b) S. Linic, P. Christopher, D. B. Ingram, *Nat. Mater.* **2011**, *10*, 911–921.
[8] a) P. Christopher, D. B. Ingram, S. Linic, *J. Phys. Chem. C* **2010**, *114*, 9173–9177; b) K. Sridharan, T. Endo, S.-G. Cho, J. Kim, T. J. Park, R. Philip, *Opt. Mater.* **2013**, *35*, 860–867.
[9] S. K. Cushing, J. Li, F. Meng, T. R. Senty, S. Suri, M. Zhi, M. Li, A. D. Bristow, N. Wu, *J. Am. Chem. Soc.* **2012**, *134*, 15033–15041.
[10] a) T. U. B. Rao, B. Nataraju, T. Pradeep, *J. Am. Chem. Soc.* **2010**, *132*, 16304–16307; b) P. Lourdu Xavier, K. Chaudhari, A. Baksi, T. Pradeep, *Nano Rev.* **2012**, *3*, 14767; c) J. Zheng, P. R. Nicovich, R. M. Dickson, *Annu. Rev. Phys. Chem.* **2007**, *58*, 409–431; d) R. Philip, P. Chantharasupawong, H. Qian, R. Jin, J. Thomas, *Nano Lett.* **2012**, *12*, 4661–4667; e) I. Chakraborty, T. Udayabhaskararao, T. Pradeep, *J. Hazard. Mater.* **2012**, *211–212*, 396–403.
[11] Y. Jin, X. Gao, *Nat. Nanotechnol.* **2009**, *4*, 571–576.
[12] W.-T. Chen, Y.-J. Hsu, P. V. Kamat, *J. Phys. Chem. Lett.* **2012**, *3*, 2493–2499.
[13] C. Yu, G. Li, S. Kumar, H. Kawasaki, R. Jin, *J. Phys. Chem. Lett.* **2013**, *4*, 2847–2852.
[14] Y. A. Attia, D. Buceta, C. Blanco-Varela, M. B. Mohamed, G. Barone, M. A. López-Quintela, *J. Am. Chem. Soc.* **2014**, *136*, 1182–1185.
[15] Y.-S. Chen, P. V. Kamat, *J. Am. Chem. Soc.* **2014**, *136*, 6075–6082.
[16] M. S. Bootharaju, T. Pradeep, *Langmuir* **2013**, *29*, 8125–8132.
[17] Y. Bu, Z. Chen, W. Li, *Appl. Catal. B* **2014**, *144*, 622–630.
[18] X. C. Wang, K. Maeda, A. Thomas, K. Takanabe, G. Xin, J. M. Carlsson, K. Domen, M. Antonietti, *Nat. Mater.* **2009**, *8*, 76–80.
[19] Y. Yang, Y. Guo, F. Liu, X. Yuan, Y. Guo, S. Zhang, W. Guo, M. Huo, *Appl. Catal. B* **2013**, *142–143*, 828–837.
[20] Y. He, J. Cai, T. Li, Y. Wu, Y. Yi, M. Luo, L. Zhao, *Ind. Eng. Chem. Res.* **2012**, *51*, 14729–14737.
[21] F. Su, S. C. Mathew, G. Lipner, X. Fu, M. Antonietti, S. Blechert, X. Wang, *J. Am. Chem. Soc.* **2010**, *132*, 16299–16301.
[22] S. Glaus, G. Calzaferri, R. Hoffmann, *Chem. Eur. J.* **2002**, *8*, 1785–1794.
[23] a) Q. Xiang, J. Yu, M. Jaroniec, *J. Phys. Chem. C* **2011**, *115*, 7355–7363; b) H. Xu, J. Yan, Y. Xu, Y. Song, H. Li, J. Xia, C. Huang, H. Wan, *Appl. Catal. B* **2013**, *129*, 182–193.
[24] S. C. Yan, Z. S. Li, Z. G. Zou, *Langmuir* **2010**, *26*, 3894–3901.
[25] a) F. A. Frame, F. E. Osterloh, *J. Phys. Chem. C* **2010**, *114*, 10628–10633; b) J. F. Reber, K. Meier, *J. Phys. Chem.* **1984**, *88*, 5903–5913.
[26] J. Yu, G. Dai, B. Huang, *J. Phys. Chem. C* **2009**, *113*, 16394–16401.

Received: January 14, 2015
Published online on ■■ ■■, 2015

FULL PAPER

Photocatalysts

K. Sridharan, E. Jang, J. H. Park, J.-H. Kim, J.-H. Lee,* T. J. Park**

■■ – ■■

Silver Quantum Cluster (Ag_9)-Grafted Graphitic Carbon Nitride Nanosheets for Photocatalytic Hydrogen Generation and Dye Degradation

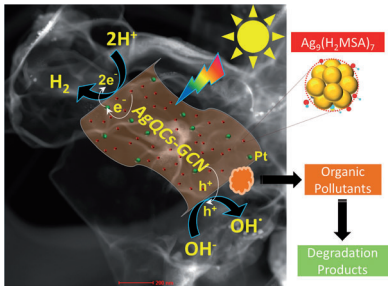

Silver metal quantum clusters embedded in graphitic carbon nitrides have been developed as new photocatalysts for environmental remediation and hydrogen evolution (see figure; Ag_9 = nine-atom silver clusters; H_2MSA = mercaptosuccinic acid; GCN = graphitic carbon nitride nanosheets).